Digital Extraction Column: Measurement and Modeling Techniques

Mark W. Hlawitschka*, Jonas Schulz, Dominic Wirz, Jan Schäfer, Alexander Keller, and Hans-Jörg Bart

The digitization of extraction columns requires a profound knowledge of the present hydrodynamics/mass transport interaction as well as appropriate measurement techniques for the detection of relevant input and target values. In this article, the different techniques for droplet size distribution as well as concentration determination are presented and new methods for online evaluation are discussed. In combination with the simulation of droplet size, holdup and solute concentration distribution, an online-capable process tool for controlling and optimizing extraction columns will be obtained.

1 Introduction

Liquid-liquid extraction, also called solvent extraction, is a classical unit operation in chemical, pharmaceutical, hydrometallurgical and biochemical industry [1–3]. The process is favored for the separation of feedstocks having low relative volatility, containing thermal instable components or having a low feed concentration. Complexation when using for instance liquid ion exchangers allows to extract metal ions from urban waste (lithium batteries recycling, electronic waste handling, etc.) [4], as well as extraction of solutes from biofeed (e.g., citric acid).

In respect to throughput, costs and footprint, extraction columns are favored. However, hydrodynamcis and mass transfer in liquid-liquid extraction columns involve a large number of variables such as coalescence of the droplets, droplet rise and backmixing effects. The state-of-the-art design procedure starts with batch experiments, mainly focusing on phase equilibria, mass transfer, physical properties and settling behavior. Miniplant and pilot plant experiments enable a detection of long-term effects, such as the accumulation of impurities, flooding behavior as well as the evaluation of the concentrations at the outlets. The pilot plant experiments are costly and can be reduced by simulation tools, considering coalescence and breakage inside the column. Monitoring droplet size distribution in combination with droplet populance models allows to simulate holdup and concentration profiles and control column and entrainment behavior. This article summarizes the recent developments in respect to measurement, monitoring and simulation of droplet behavior in extraction columns (see Fig. 1).
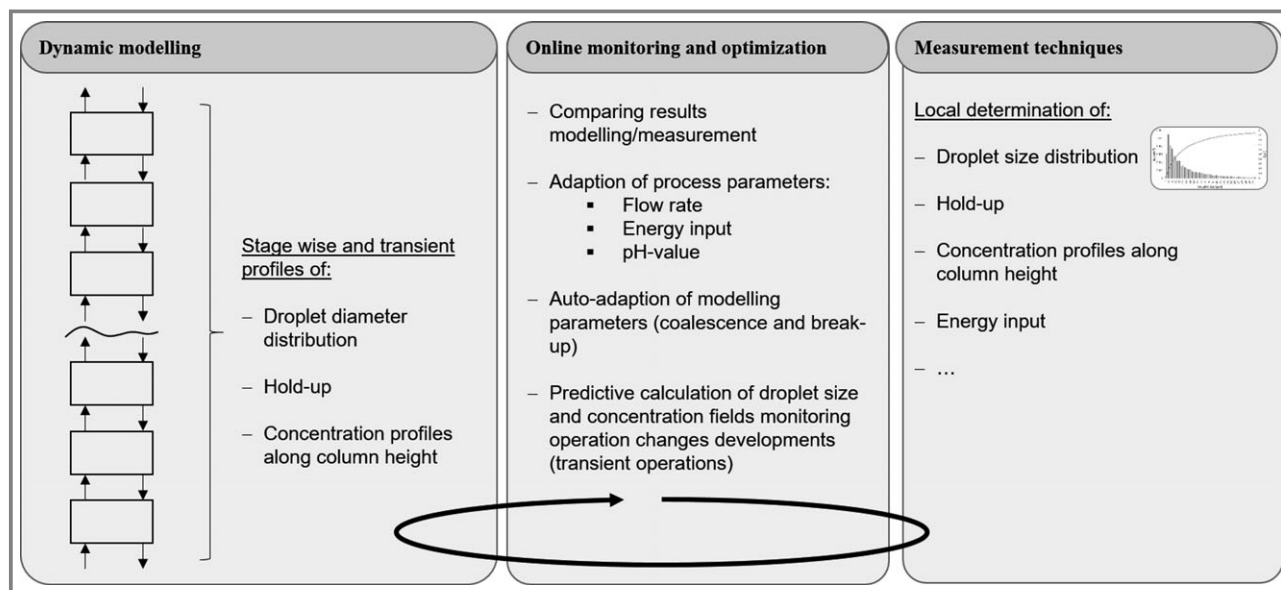
2 Particle Measurement Techniques

Hydrodynamics influence droplet behavior and interaction directly and by that exert a crucial effect on mass transfer and phase settling behavior. In order to simulate and predict column performance or entrainment rates, the knowledge of a change of intrinsic properties, like droplet size distributions (DSD) is required in order to describe the full process. Literature lists a variety of different measurement techniques that can be distinguished in offline/atline, online and inline principles [5] – independent of the measurement principle.

The DSD can also be measured with optical [6], absorption, conductivity [7] or laser-based methods like focus beam reflectance measurement [8, 9]. Online methods analyze ideally an isokinetic bypass flow and in contrast, inline techniques are placed inside the apparatus, usually executed as probes. An alternative classical measurement principle is the needle probe that is inserted in the apparatus. A thin tip containing electrodes allows the penetration of droplets measuring the chord length. An information about chord lengths gives trends of a transient process behavior, but the true DSD cannot be derived. However, there are approaches for its estimation, but they fail to work with non-spherical

Dr.-Ing. Mark W. Hlawitschka, Jonas Schulz, Dominic Wirz, Jan Schäfer, Alexander Keller, Prof. Dipl.-Ing. Dr. techn. Hans-Jörg Bart
mark.hlawitschka@mv.uni-kl.de, mark.hlawitschka@jku.at
Technische Universität Kaiserslautern, Chair of Separation Science and Technology, Postfach 3049, 67663 Kaiserslautern, Germany.

Figure 1. Interaction of modeling, online monitoring and measurement techniques.

particles and multimodal distributions [9–12]. Other laser methods, like phase Doppler anemometry (PDA), are good to detect particle velocities but size evaluation is limited to the submillimeter range. However, this is good for sprays but not really applicable with liquid droplets in the millimeter range [13].

In the last decade, process control in industry with digital cameras and application of imaging methods was an economic success [14]. The technology offers various ways in the measurement of droplets, with either incident or transmitted light, where the latter is also known as shadowgraphy [15]. Additionally, the imaging techniques can be distinguished in the type of lens used, namely entocentric, telecentric and hypercentric lenses [5]. The most used lense is entocentric and the imaging works like the human eye. Most measurement probes eliminate the disadvantage of distance-dependent imaging by using a small focal plane where the particles appear sharp and their size can be accurately determined, leading unfortunately to a small measurement volume [16, 17]. A few companies commercially offer probes applying incident light, e.g., Mettler Toledo Inc. [8], Pixact Ltd. [18] or SOPAT GmbH [19]. Further, various online microscopes (Sympatec GmbH) are commercially available using a transmitted light approach and can be operated as online measurement in a bypass flow.

Telecentric lenses became more popular in the recent years, as they allow distance-independent imaging of objects. In addition, they span a relatively high depth of field compared to entocentric lenses [20], leading to a wider measurement volume, thus, a higher yield of particles per image. Larger outer dimensions and higher light intensity are the main disadvantages of this measurement technique. Telecentric lenses are about 4 to 8 times larger than probes deploying an entocentric lens [21]. Hypercentric lenses

acquire multiple sides of one object at once but are not applied for particle detection in chemical engineering by now.

A combination of transmitted light and telecentric illumination with a telecentric lens has been recently published [22]. This setup achieves high contrast images and a precise particle size analysis, independent on their position within the measurement volume. Initially, the measurement system was placed in a measurement cell comprising two vis-a-vis units, which contain camera and illumination, respectively. With a focus on miniplant and laboratory scale, these cells have been adapted from DN 25 up to DN 450 with a detection range of 10 µm up to 20 mm depending on the lenses applied. A combination of this setup with an online analysis tool allows droplet detection up to 25 % holdup with an accuracy of 5 % [15]. A priory calibration of the optical probe is not necessary, because the calibration factor is constant in one telecentric setup. The measurement range and accuracy can be extended to higher values by using lenses with lower magnification and sensors with higher resolution by equivalent sensor size. For industrial application, an endoscopic one-sided probe containing the two-sided measurement principle represents a solution for apparatuses bigger than DN 450 [23, 24]. This concept is easily integrated via a DN 50 / DN 80 flange and flexible by adjusting the measurement volume and position without unmounting the probe. This measurement principle is successfully applied in mixer-settlers [25], extraction columns [26], pumps and pipes [27]. Furthermore, measurements in bubble columns allow a determination of the interfacial area [28], even in slurry bubble columns with the presence of solid particles, such as catalysts [29]. While all these fluid systems contain a liquid continuous phase, modifications in probe design also enable spray detection [30, 31]. In

conclusion, there are several measurement techniques that can be used to detect droplets in a continuous phase, having different advantages and disadvantages as summarized in Tab. 1.

3 Image Analysis

DSD measurements acquired by camera-based optical imaging approaches require postprocessing operations to extract the features of interest, e.g., Sauter mean diameter, from the captured data. The challenges of this approach are operations at high holdup, where particles or droplets overlap or occlude each other. This can be especially observed for the operation points in extraction columns, where holdup reaches up to 25–30 %. The postprocessing can be split into two different procedures, the segmentation of overlapping particles and the feature extraction of the separated particles, e.g., diameter. For the segmentation task, there are different solutions to this problem, ranging from algorithms specifically designed for this case, up to machine learning approaches. Tab. 2 shows an overview of different methods.

Each of the measurement techniques has its advantages and disadvantages. Their applicability depends on the operational conditions. A well-known example for an algorithm is the marker-based watershed, where a binary image is segmented into neighboring areas of interest by first finding the appropriate regional markers, (distance transform and ultimate erosion) and then growing these regions until they touch. These contact points are the basis for the segmentation of the areas [44].

Machine learning approaches enable a flexible adaption of the segmentation procedure, by training the model for the specific scenario. A variant of convolutional neural networks, U-net introduced by Ronneberger et al. [43], allows a local segmentation of objects in images. The network was

Table 1. Measurement techniques for droplet size distributions (c = continuous, d = disperse).

Author	Column	Fluid system	Measurement technique	Measurement principle	Particle size range [mm]
Asadollahazadeh et al. [32]	Scheibel® column, D = 113 mm	water (c), n-butanol (d), toluene (d), n-butyl acetate (d)	imaging, digital camera, incident light	offline	0.5–5
Amokrane et al. [19]	pulsed disc and doughnut, D = 25 mm	hydrogenated tetrapropylene (c), water (d); and hydrogenated tetrapropylene mixture with Marcol (oil) (c)	imaging, SOPAT-VF, probe, incident light	inline	0.02–2
Yi et al. [33]	pulsed packing column (ceramic sieves, ceramic structured packings), D = 72 mm	tap water (c), tributyl phosphate (d)	imaging, digital camera, incident light	offline	0.5–4
Xi et al. [34]	pulsed sieve plate column, D = 38 mm	water (c), kerosene (d)	trisensor needle probe	inline	1–4
Mickler et al. [15]	stirred cell column, D = 150 mm	water (c), isododecane (d)	imaging, transmitted and incident light, probe	inline	0.02–7
Gholam Samani et al. [35]	pulsed packing column (Raschig rings), D = 55 mm	water (c), kerosene(d), n-butyl acetate (d)	imaging, digital camera, incident light	offline	0.5–5
Torab-Mostaedi et al. [36]	pulsed packing (Raschig rings) column, D = 76 mm	water (c), toluene (d), n-butyl acetate (d)	imaging, digital camera, incident light	offline	1–3.5
Usman et al. [37]	pulsed sieve-plate column, D = 55 mm	water (c), kerosene-benzoic acid solution (d)	imaging, digital camera, incident light	offline	1–6
Steinmetz [38]	Kühni column, D = 32 mm	water (c), n-butyl acetate (d), toluene (d)	imaging, transmitted light, suction probe	inline, online	0.3–7
Lorenz et al. [39]	pulsed sieve plate column, D = 80/225 mm	water (c), n-butanol (d), toluene (d), n-butyl acetate (d)	photoelectric suction detector	inline	2–8
Korchinsky and Al-Husseini [40]	Rotating disc contator D = 219 mm	water (c), toluene (d)	imaging	offline	3–50
Grag and Pratt [41]	Pulsed sieve-plate column D = 72 mm	water (c), methyl isobutyl ketone (d)	imaging, digital camera, incident light	offline	0.4–2

Table 2. Segmentation techniques (c = continuous, d = disperse).

Author	Fluid system	Measurement technique	Software: segmentation technique
Schäfer et al. [42]	water (c), paraffin oil (d)	imaging, transmitted light probe	Python (pytorch): Convolutional neural network (U-net [43])
Lichti et al. [28]	water (c), air (d)	imaging, transmitted light probe	Tool IP (Fraunhofer): Watershed
Amokrane et al. [26]	hydrogenated tetrapropylene (c), water (d)	imaging, SOPAT-VF, incident light probe	SOPAT: pattern recognition, pre-selection of plausible circle positions, classification by edge examination
Mickler et al. [15]	water (c), isododecane (d)	imaging, transmitted and incident light probe	Matlab: Random forest classifier, Distance transform + Watershed, Hough circle transform, Template matching, Random sample consensus
Maaß et al. [16]	water (c), petroleum (d), water (c), n-butyl chloride (d)	imaging, incident light probe	Matlab: pattern recognition, pre-selection of plausible circle positions, classification by edge examination
Torab-Mostaedi et al. [42]	water (c), toluene (d), n-butyl acetate (d)	imaging, digital camera, incident light	AutoCAD: Manual segmentation

designed for biological image segmentation, but its application is not limited to this field of work. The network can be trained to segment different objects of interest. The main problem in this case is that a training database with already evaluated data is required. In most cases such an extensive database does not exist. Schäfer et al. [42] present a solution using computer generated imaging data, which can be easily adapted for different cases in particulate systems when applying the OMOP camera system [21, 45].The trained network can be used to generate a database of segmented images to train a second network on segmenting the original images without preprocessing them (see Fig. 2).

A further part of the evaluation procedure is to allocate to each segmented contour the correct particle size. In the most common case, with spherical droplets, a diameter can be derived from a minimal enclosing circle fixed at three extreme points of the contour. For nonspherical droplets with an ellipsoidal (oblate or prolate) shape, more assumptions are needed to assign a measurement value. The final fitting of an ellipse to a contour can be done using a minimization algorithm, which finds the minimal distance between all contour points and the fitted ellipse [46].

4 Simulation Techniques

An extraction column simulation with a plug flow model or the cell model is roughly applicable with pulsed columns but with stirred columns backmixing effects cannot longer be neglected. A more sophisticated model by Casamatta and Vogelpohl [6] considered breakage and coalescence of droplets in a droplet population balance model (DPBM). It is based on the definition of the function n, which represents the number distribution of the droplet size in a specific section of the extraction column:

$$\frac{\partial n_{d,c_y}(\Psi)}{\partial t} + \frac{\partial\left[u_d n_{d,c_y}(\Psi)\right]}{\partial z} + \frac{\partial\left[\dot{c}_y n_{d,c_y}(\Psi)\right]}{\partial c_y}$$
$$= \frac{\partial}{\partial z}\left[D_{ax,y}\frac{\partial n_{d,c_y}(\Psi)}{\partial z}\right] + \frac{Q_y^{in}}{A_c}n_y^{in}(d_m, c_y; t)\delta(z - z_d) + \Theta\{\Psi\}$$

(1)

The first term on the left side of Eq. (1) represents the transient term for the change in the drop density function per unit time. The second term represents the convection
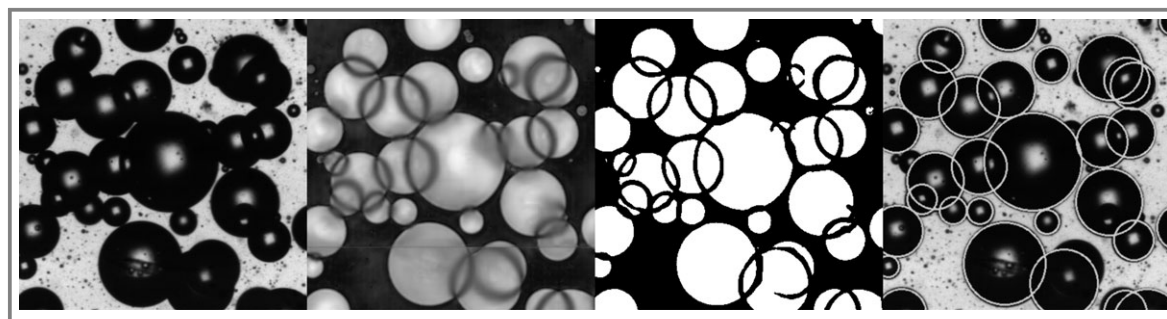
Figure 2. Image analysis steps using U-net for image segmentation.

term along the external coordinates for the drop movement. The phase velocity of the disperse phase u_d is determined with regard to the relative velocity. The third term represents convection along the internal coordinates for the diffusion term. The mass transfer process between the contacted phases can be related to the convective mass transfer from the continuous phase. Based on this, the rate of change of the dissolved concentration in each drop is given by [47]:

$$\dot{c}_y = \frac{\partial c_y(z,t)}{\partial t} = \frac{6k_{oy}}{d}\left(c_y^*(c_x) - c_y(z,t)\right) \qquad (2)$$

where k_{oy} is the overall mass transfer coefficient, m is the partition coefficient, c_y is the concentration in the disperse phase and c_x is the concentration in the continuous phase. The total mass transfer coefficient can be calculated using the two-film theory.

On the right side of Eq. (1) are the source terms. The first source term describes the axial dispersion of the drops, which refers to the change in flow due to random movements of the drops. It is characterized by the axial dispersion coefficient $D_{ax,y}$, which depends on the energy dissipation and the droplet rise velocity. The second source term expresses the drop entry rate into the liquid-liquid extraction column. The third source term Θ represents the net number of drops generated by breakage and coalescence per unit volume and time. The source term Θ is determined by the four rates of drop birth (B) and death (D) due to breakage (b) and coalescence (c):

$$\Theta\{\Psi\}$$
$$= B^b(d, c_y; t, z) - D^b(d, c_y; t, z) + B^c(d, c_y; t, z) \qquad (3)$$
$$- D^c(d, c_y; t, z)$$

The four rates are determined by a series of equations shown in Tab. 3 [48].

An overview in respect to numerical solution methods and its application with extraction columns is given else-

where [49]. Moment-based methods allow online simulations and a coupling with CFD (computational fluid dynamics) codes due to their low computational load. For instance, the One Primary One Secondary Particle Method (OPOSPM) [50] or Interfacial Area Transport Equation (IATE) [51] are able to track the droplet population balance with only one single equation. In the OPOSPM, the source term can be further simplified to a nonintegral description:

$$\Theta = (\vartheta(d_{30}) - 1)\Gamma(d_{30})n_d - \frac{1}{2}\omega(d_{30}, d_{30}) \qquad (4)$$

The first term is the drop generation due to drop breakup and includes the breakage frequency Γ. In addition, the number of daughter droplets is accounted by $\vartheta(d_{30})$. The second term describes the net rate of droplets which are removed from the balance due to coalescence and includes the coalescence frequency ω. Both frequencies are dependent on the density, viscosity and interfacial tension.

4.1 Correlations and Parameters

For the closure of the DPBM, a set of correlations is required, e.g., for droplet velocity, droplet breakage and coalescence and axial dispersion, to obtain a reasonable description of the column. The most common correlations for single droplet rise are given in Tab. 4 and slowing factors for the droplet swarm in a certain geometry is listed in Tabs. 5 and 6. A full overview on the available correlations is given by Bart et al. [49].

4.2 Mass Transfer

The correlations for mass transfer coefficients based on the two-film theory are given in Tab. 7. However, at high initial solute concentrations, the mass transfer is highly influenced by Marangoni convection, inducing a surface renewal and finishing 80 % of mass transfer directly after drop formation [61]. Therefore, further extensions of the correlations are required.

5 Concentration Measurement Techniques

In order to predict extraction efficiency of a separation problem the knowledge of an axial solute profile is essential [66]. Several measurement techniques are summarized in Tab. 8. Sum parameters such as density, refractive index,

Table 3. Breakage and coalescence rates.

Source term	Rate
B^b	$\displaystyle\int_d^{d_{max}}\int_0^{c_{y,max}}\Gamma(d',\varphi_y,P)\beta_n(d|d')n_{d,c_y}(d',c_y';t,z)\delta(c_y'-c_y)\partial d'\partial c_y'$
D^b	$\Gamma(d',\varphi_y,P)n_{d,c_y}(d,c_y;t,z)$
B^c	$\displaystyle\frac{1}{2}\int_0^d\int_{c_{y,min}'}^{c_{y,max}'}\omega(d',\eta,\varphi_y,P)\left(\frac{d}{\eta}\right)^5 n_{d,c_y}(d',c_y';t,z)n_{d,c_y}(\eta,c_y'';t,z)\partial d'\partial c_y' \text{ with } \eta = (d^3-d'^3)^{1/3}$
D^c	$n_{d,c_y}(d,c_y;t,z)\displaystyle\int_0^{(d_{max}^3-d^3)^{\frac{1}{3}}}\int_0^{c_{y,max}}\omega(d,d',\varphi_y,P)n_{d,c_y}(d',c_y';t,z)\partial d'\partial c_y'$

© 2020 The Authors. Published by WILEY-VCH Verlag GmbH & Co. KGaA, Weinheim

Table 4. Droplet rise velocity correlations from literature.

Author	Correlation	Range of validity
Rigid sphere law [52]	$u_t = \left(\left(\frac{g \Delta \rho d^2}{18 \eta_x} \right)^{-0.85} + \left(1.74 \sqrt{\frac{g \Delta \rho d}{\rho_x}} \right)^{-0.85} \right)^{-\frac{1}{0.85}}$	$10^{11} < \frac{1}{Mo}$
Vignes [53]	$u_t = \left(\frac{\rho_x}{\eta_x} \right)^{\frac{1}{3}} \left(\frac{g \Delta \rho}{\rho_x} \right)^{\frac{2}{3}} \left(\frac{1 - E\ddot{o}}{6} \right) \left(\frac{d}{4.2} \right)$	$10^7 < \frac{1}{Mo} < 10^{11}$
Klee and Treybaal [54]	For $d < d_{crit}$: $u_t = 38.3 \rho_x^{-0.45} \Delta \rho^{0.58} \eta_x^{-0.11} d^{0.7}$ For $d > d_{crit}$: $u_t = 17.6 \rho_x^{-0.55} \Delta \rho^{0.28} \eta_x^{-0.1} \sigma^{0.18}$ with: $d_{crit.} = 0.3 \rho_x^{0.14} \Delta \rho^{-0.43} \eta_x^{0.3} \sigma^{0.24}$	$10^5 < \frac{1}{Mo} < 10^7$
Grace et al. [55]	$u_t = \frac{\eta_x}{d \rho_x} Mo^{-0.149} (J - 0.857)$ $J = \begin{cases} 0.94 H^{0.757} \text{ for}: 2 < H < 59.3 \\ 3.42 H^{0.441} \text{ for}: H > 59.3 \end{cases}$ $H = \frac{4}{3} E\ddot{o} Mo^{-0.149} \left(\frac{\eta_x}{\eta_{Water}} \right)$	$\frac{1}{Mo} < 10^5$

Table 5. Correlations for slowing factors.

Author	Correlation	Range of validity
Fang et al. [56]	$k_V = 1 - \left[\frac{(1 - \varphi_S) \left(\frac{s_1 Re_D}{\varphi_S} \right)}{1 + \left(\left(\frac{s_1 Re_D}{\varphi_S} \right) \right)} \right]$	Kühni column, $D = 152$ mm, turbine agitator; different test systems $Re_D > 3000$
Modes [57]	$k_V = 1 - 0.137 Re_D^{0.156}$	RDC column, $D = 150$ mm; water, toluene
Schmidt [58]	$k_V = 1 + s_1 N_P^{s_2} + s_3 \left(\frac{d}{D_C - D_S} \right)^{s_4} + s_5 \left(\frac{H_c}{D_C} \right)^{s_6} + s_7 \varphi_S^{s_8}$	Kühni column, $D = 152$ mm, turbine agitator; different test systems
Steinmetz [38]	$k_V = \frac{D_s - D_R}{d} s_1 + s_2 \frac{D_c}{H_c} exp \left(-s_3 \left(\frac{N_P - s_4}{s_5} \right)^2 \right)$	Kühni column, $D = 32$ mm

Table 6. List of parameters used for the slowing factor determination.

Author	s_1	s_2	s_3	s_4	s_5	s_6	s_7	s_8
Fang et al. [56]	$7.18 \cdot 10^{-5}$	–	–	–	–	–	–	–
Garthe [59]	−1.669	−3.945	−2.807	1.336	−1.159	2.049	2.1	1.032
Garthe adapted by Jildeh [48]	−1.9104	−2.621	−58.55	$3.70 \cdot 10^{-3}$	−0.290	2.956	58.9154	$4.20 \cdot 10^{-3}$
Schmidt [60]	−1.5	−3.18	−145.26	3.26	−22.07	9.98	1.35	0.94
Steinmetz [38]	0.0028	0.7227	0.5	1.703	0.3105	–	–	–
Steinmetz adapted by Jildeh [48]	$3.90 \cdot 10^{-3}$	0.696	0.492	1.819	0.431	–	–	–

conductivity can also be used for online monitoring. Direct UV/Vis spectroscopy reaches its limits when several absorbing components are present. In this case, the mixture of compounds must be separated by liquid or gas chromatography. With complex separation tasks more sophisticated analytics can be applied, like Fourier-transformed infrared spectroscopy (FTIR) or attenuated total reflection technology (ATR), while the latter enables inline measurements. Atomic absorption spectroscopy (AAS) or atomic emission spectroscopy for multi-element analysis (AES) are methods to quantify metal ions in aqueous phase or metal complexes in the organic phase. Typical detection limits are in the range of $1 \, ng \, L^{-1}$ to $1000 \, \mu g \, L^{-1}$.

Table 7. Common applied mass transfer correlations.

Author	Correlation	Range of validity
Garner and Tayeban [62]	$k_x = \dfrac{D_x}{d}\left(2 + 0.67\sqrt{Re_o Sc_x}\right)$	Rigid sphere
Kronig and Brink [63]	$k_x = \dfrac{D_x}{d}\left(0.6\sqrt{Re_o Sc_x}\right)$	Circulating droplet
Treybal [64]	$k_x = \dfrac{D_x}{d}\left(0.725 Re_o^{0.57} Sc_x^{0.42}\left(1 - \varphi_y\right)\right)$	Circulating droplet
Heertjes [65]	$k_x = 0.83\sqrt{\dfrac{D_x u_r}{d}}$	Oscillating droplet

Table 8. Solute (s) measurement techniques in dispersed (d) and continuous (c) phases (t = transfer component).

| Author	Apparatus	Fluid system	Concentration measurement technique	Inline/Online/ Offline
Korb et al. [67]	Kuehni column, $D = 32$ mm	zinc (s) in water (c); D2EHPA* in isododecane/(d)	AAS	offline
Kolhe et al. [68]	pulsed sieve plate column, $D = 76.2$ mm	KCl (s) in water (c)	conductivity probe	inline
Nishi et al. [69]	microfluidic device	cobalt (s) in water (c)/D2EHPA in decane (c)	UV/Vis	inline
Jahya et al. [70]	pulsed disc & doughnut column, $D = 72.5$ mm	Water (c)/ toluene (d) acetone (s); Alamine336** in Shellsol 2046*** (c) sulfuric acid (s) in water (d)	UV/Vis	online
Torab-Mostaedi and Safdari [71]	packed column, ceramic Raschig rings, $D = 50$ mm	Water (c)/toluene (d) or n-butyl-acetate(d)/ acetone (s)	gas chromatograph (MXT-1) with flame ionization detector	offline
Tsouris and Tavlarides [72]	Oldshue-Rushton column, $D = 125$ mm	water (c)/toluene (d)/butyric acid (s)	conductivity cell (Yellow Springs Instrument Co., Inc., YSI Model 32)	online
Korchinsky and Al-Husseini [40]	RDC, $D = 219$ mm	water (c)/toluene (d); acetone (s)	chromatography (Pye Unicam Series 604)	online
Bonnet and Jeffreys [66]	4-blade turbine extraction column, $D = 100$ mm	water (c)/toluene (d); acetone (s)	sample collector system for turbulent flow	offline

*D2EHPA = Di(2ethylhexyl)phosphoric acid is a liquid cation exchanger; ** Alamine 336 is a liquid anion exchanger; ***Shellsol 2046 is a kerosene like solvent.

6 Predictive Online Monitoring

Predictive online monitoring starts with a reliable and validated set of equations. To obatin these, a three-step approach was presented by Jildeh [48]. The first step is based on the parameter optimization of existing single droplet literature correlations for velocity, slowing factor and breakage probability using single droplet measurements or CFD simulations. The second step involves the determination of the energy dissipation and axial dispersion correlations using CFD tools [48, 73–75], which allow a good determination of these parameters also for industrial-sized columns, where correlations are rare. In the third place, solving an inverse population balance approach together with swarm experimental data obtained from lab-scale col-

umns enables a determination of the required coalescence parameters. The three-step approach enables a decrease of complexity of the highly interacting multiphase problem. Therefore, a robust simulation can be set up for online monitoring.

As an example, model combinations using different slowing factors are shown in Fig. 3. In general, with a validated set of correlations, a good agreement to experimental data can be achieved regarding holdup, droplet size and concentration profiles in the continuous as well as in the disperse phase. Taking the validated set of equations, combining them to image analysis or other measurement techniques, predictive online monitoring of the whole extraction process is possible [48, 76, 77]. Furthermore, this can be used to analyze the influence of flow rate changes and energy input
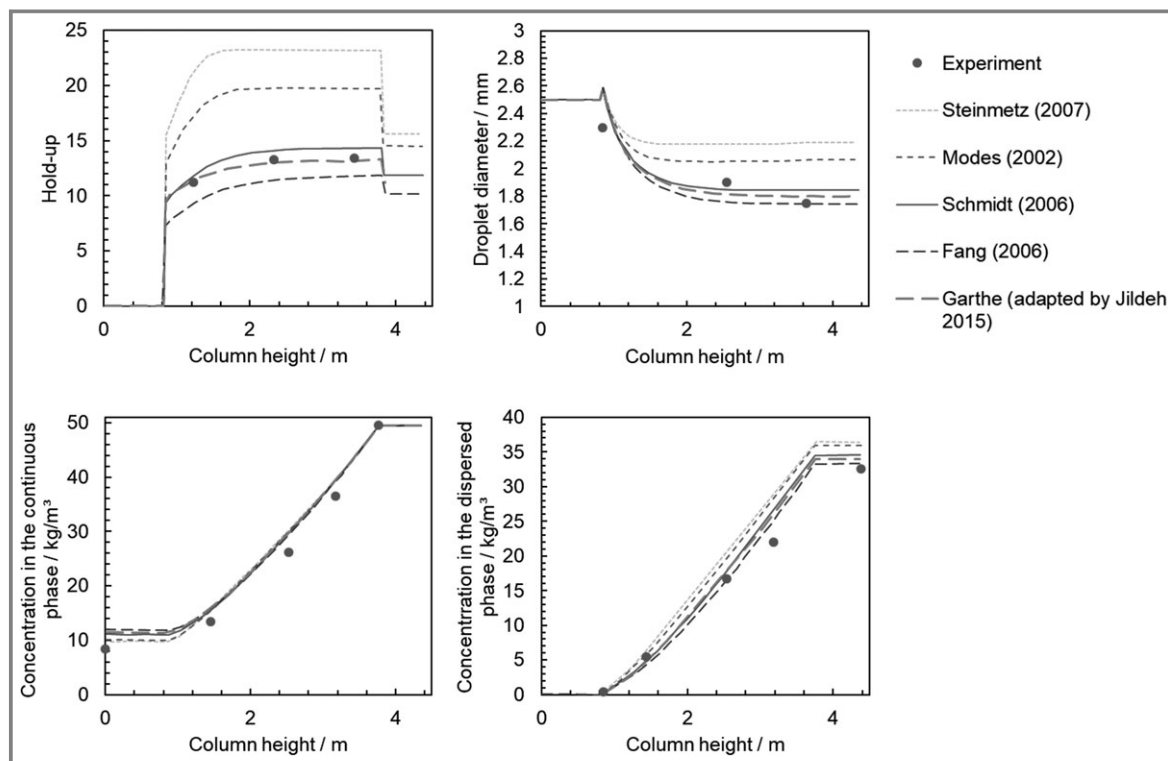
Figure 3. Influence of correlation sets of slowing factors compared to experimental data of Garthe [57]. Column type Kühni: Continuous flow rate: 40 L h^{-1}, dispersed flow rate: 48 Lh^{-1}, rotational speed: 100 rpm; system: butyl acetate/acetone/water.

in regard to, e.g., concentration or holdup profiles. These predictions enable an operational control of a process. Thus, control of flooding or entrainment rates of a regulated or given raffinate solute concentration, is possible [45].

7 Summary and Outlook

The future of digitalization in process industry relies on adequate measurement techniques, robust modeling and simulation approaches and the generation of suitable online tools, together with well-trained operators. Therefore, not only experts in a single field are necessary, the expertise must spread among all associated fields [78].

In this review, the recent developments of measurement techniques concerning droplet size and concentration fields in extraction columns are collected. With particle image analysis the trend from particle segmentation by classical watershed algorithms towards neural networks is highlighted. 3-D CFD simulation and single droplet experiments can help to identify reasonable 1-D correlations, not only for mini- and pilot plant, but also for the larger industrial-scale columns. With the implementation of predictive online monitoring tools into industrial application, operational failures can be monitored, analyzed and reduced as well as the optimum operation point can be automatically set, based on appropriate inline input data.

Mark W. Hlawitschka studied at TU Kaiserslautern Mechanical and Process Engineering. In 2013, he finished his PhD thesis with distinction at the chair "Thermische Verfahrenstechnik" in the field of liquid-liquid extraction. He decided to focus on gas-liquid systems and established a research group at TU Kaiserslautern on this topic. He was elected chairman of "TU Nachwuchsring" during 2017–2020. In 2019, he received his habilitation in the field of Thermal Process Engineering. In October 2020, he will start his professorship at JKU Linz in the field of Chemical Process Engineering.

Jonas Schulz studied Industrial Engineering with focus on Process Engineering at the TU Kaiserslautern, Germany and Linköpings universitet (li.u), Sweden. After his graduation (B.Sc. 2014; M.Sc. 2016) he started to work as a research associate at the chair of "Thermische Verfahrenstechnik" under the supervision of Prof. Hans-Jörg Bart. His field of research comprises optical measurement techniques for application in chemical plants, fluid mechanics and droplet separation particularly liquid entrainment from trays and packings.

Dominic Wirz finished an apprenticeship in metal working in 2007 and extended his education with a degree as certified technician for mechanical construction from Handwerkskammer des Saarlandes in 2010. He worked one year as a chief constructor at Eliseo Hummer GmbH before he began his study at the TU Kaiserslautern. After graduation in Mechanical Engineering (diploma, 2017), he started his PhD at the chair of "Thermische Verfahrens-

technik". He focuses on optical measurement methods for the evaluation of particulate properties in multiphase flows with objective of graduation (Dr.-Ing) in 2022.

Jan Schäfer, born 1987, graduated in Business Economics, with specialization in Chemical Engineering, at the TU Kaiserslautern. Since 2016, he is working towards his doctoral degree at the "Thermische Verfahrenstechnik" of Prof. Hans-Jörg Bart. He is expert in Computational Fluid Dynamics and interested in neuronal networks and machine learning. He will finish his PhD in 2020.

Alexander Keller is a skilled chemistry laboratory assistant. After his apprenticeship, he studied Process Engineering and Chemical Engineering at Clausthal University of Technology and TU Kaiserslautern. In 2018, he started as PhD student at the chair "Thermische Verfahrenstechnik" at TU Kaiserslautern. He is working on recycling processes for lithium ion batteries with focus on reactive solvent extraction.

Hans-Jörg Bart studied chemical engineering and received his doctoral degree at the University of Technology, Graz, Austria. After his professorial thesis (habilitation) he was head of the Christian Doppler Laboratorium "Modellierung Reaktiver Systeme in der Verfahrenstechnik" and is now a "Senior Fellow" of the Christian-Doppler-Society, Vienna. He is Honorary Professor at Kumning University, China and since 1994 he is chairing "Thermische Verfahrenstechnik" at TU Kaiserslautern.

Symbols used

A_c	$[\text{m}^2]$	column cross-sectional area
B^b	$[\text{m}^{-3}\text{s}^{-1}]$	breakage source term due to birth
B^c	$[\text{m}^{-3}\text{s}^{-1}]$	coalescence source term due to birth
c_x	$[\text{kg m}^{-3}]$	solute concentration in the continuous phase
c_y	$[\text{kg m}^{-3}]$	solute concentration in the disperse phase
$c_y^{\ *}$	$[\text{kg m}^{-3}]$	solute equilibrium concentration at the interface
D^b	$[\text{m}^{-3}\text{s}^{-1}]$	breakage source term due to death
D^c	$[\text{m}^{-3}\text{s}^{-1}]$	coalescence source term due to death
d	$[\text{m}]$	droplet diameter
d'	$[\text{m}]$	daughter droplet diameter
d_{30}	$[\text{m}]$	volume mean diameter
d_{32}	$[\text{m}]$	Sauter mean diameter
D_{ax}	$[\text{m}^2\text{s}^{-1}]$	axial dispersion
D_c	$[\text{m}]$	column width
D_x	$[\text{m}^2\text{s}^{-1}]$	diffusion coefficient continuous phase
D_R	$[\text{m}]$	rotor diameter
D_S	$[\text{m}]$	shaft diameter
$E\ddot{o}$	$[-]$	Eötvös number, $\dfrac{g\Delta\rho d^2}{\sigma}$
g	$[\text{m s}^{-2}]$	gravitational acceleration
H_c	$[\text{m}]$	compartment height
k_{oy}	$[\text{m s}^{-1}]$	overall mass transfer coefficient
k_V	$[-]$	slowing factor
Mo	$[-]$	Morton number, $\dfrac{g\Delta\rho\eta_x^4}{\rho_x^2\sigma^3}$
n_d	$[\text{m}^{-3}\text{s}^{-1}]$	total number of droplets
N_P	$[-]$	Power number, $\dfrac{P}{n^3 D_R^5 \rho_x}$
n_y^{in}	$[\text{m}^{-3}\text{s}^{-1}]$	number of droplets (inlet)
P	$[\text{m}^{-1}]$	volumetric distribution density
Q_y^{in}	$[\text{m}^3\text{s}^{-1}]$	volumetric flow rate
Re	$[-]$	droplet Reynolds number, $\dfrac{\rho_x d u}{\eta_x}$
Re_R	$[-]$	rotor Reynolds number, $\dfrac{\rho_c D_R^2 N}{\eta_x}$
$s_1 \dots s_8$	$[-]$	parameters
Sc_x	$[-]$	Schmidt number of the continuous phase, $\dfrac{\eta_x}{\rho_x D_x}$
t	$[\text{s}]$	time
u_d	$[\text{m s}^{-1}]$	disperse phase velocity
u_r	$[\text{m s}^{-1}]$	relative velocity
u_t	$[\text{m s}^{-1}]$	terminal velocity
z	$[\text{m}]$	space coordinate

Greek symbols

β_n	$[\text{m}^{-1}]$	daughter droplet distribution based on droplet number
Γ	$[\text{s}^{-1}]$	breakage rate
η	$[\text{kg m}^{-1}\text{s}^{-1}]$	dynamic viscosity
Θ	$[\text{s}^{-1}]$	source term
ϑ	$[-]$	number of daughter droplets
ρ	$[\text{kg m}^{-3}]$	density
φ_S	$[-]$	phase fraction
Ψ	$[-]$	internal and external coordinate vector $[d,c_y,z,t]$
ω	$[\text{m}^3\text{s}^{-1}]$	coalescence rate

Abbreviations

CFD	computational fluid dynamics
CNN	convolutional neural network
DPBM	droplet population balance model
DSD	droplet size distribution
OMOP	optical multimode online probe
SMD	Sauter mean diameter
DN	nominal diameter

References

[1] C. Hanson, *Recent advances in liquid-liquid extraction*, Pergamon Press, Oxford **1971**.

[2] R. Schmidt, *Chem. Ing. Tech.* **1988**, *60 (12)*, 956–965. DOI: https://doi.org/10.1002/cite.330601205

[3] J. Rydberg, M. Cox, C. Musikas, *Solvent extraction principles and practice*, Marcel Dekker, Hoboken **2004**.

[4] S. Virolainen, M. Fallah Fini, A. Laitinen, T. Sainio, *Sep. Purif. Technol.* **2017**, *179*, 274–282. DOI: https://doi.org/10.1016/j.seppur.2017.02.010

[5] M. Lichti, H.-J. Bart, *ChemBioEng Rev.* **2018**, *5 (2)*, 79–89. DOI: https://doi.org/10.1002/cben.201800001

[6] J. M. Delhaye, O. C. Jones, *A Summary on experimental methods for statistical transient analysis of two-phase gas-liquid flow*, report, Argonne National Laboratory, Argonne, IL June **1976**.

[7] S. C. Saxena, D. Patel, D. N. Smith, J. A. Ruether, *Chem. Eng. Commun.* **1988**, *63 (1)*, 87–127.

[8] P. Barrett, B. Glennon, *Chem. Eng. Res. Des.* **2002**, *80 (7)*, 799–805.

[9] A. Ruf, J. Worlitschek, M. Mazzotti, *Part. Part. Syst. Charact.* **2000**, *17 (4)*, 167–179. DOI: https://doi.org/10.1002/1521-4117(200012)17:4<167:AID-PPSC167>3.0.CO;2-T

[10] N. N. Clark, R. Turton, *Int. J. Multiphase Flow* **1988**, *14 (4)*, 413–424.

[11] E. F. Hobbel, R. Davies, F. W. Rennie, T. Allen, L. E. Butler, E. R. Waters, J. T. Smith, R. W. Sylvester, *Part. Part. Syst. Charact.* **1991**, *8 (1–4)*, 29–34.

[12] M. J. H. Simmons, P. A. Langston, A. S. Burbidge, *Powder Technol.* **1999**, *102 (1)*, 75–83.

[13] K. Bauckhage, *Chem. Ing. Tech.* **1996**, *68 (3)*, 253–266. DOI: https://doi.org/10.1002/cite.330680306

[14] M. Schlüter, *Chem. Ing. Tech.* **2011**, *83 (7)*, 992–1004.

[15] M. Mickler, B. Boecker, H.-J. Bart, *Flow Meas. Instrum.* **2013**, *30*, 81–89. DOI: https://doi.org/10.1016/j.flowmeasinst.2013.01.004

[16] S. Maaß, J. Rojahn, R. Hänsch, M. Kraume, *Comput. Chem. Eng.* **2012**, *45*, 27–37. DOI: https://doi.org/10.1016/j.compchemeng.2012.05.014

[17] S. Maaß, S. Wollny, A. Voigt, M. Kraume, *Exp. Fluids* **2011**, *50 (2)*, 259–269. DOI: https://doi.org/10.1007/s00348-010-0918-9

[18] R. Kopra, H. Mutikainen, O. Dahl, *Tappi J.* **2018**, *17 (6)*, 339–346.

[19] A. Amokrane, S. Maaß, F. Lamadie, F. Puel, S. Charton, *Chem. Eng. J.* **2016**, *296*, 366–376. DOI: https://doi.org/10.1016/j.cej.2016.03.089

[20] R. Schuhmann, T. Thöniß, *Tech. Mess.* **1998**, *65 (4)*, 131–136.

[21] H.-J. Bart, M. W. Hlawitschka, M. Mickler, M. Jaradat, S. Didas, F. Chen, H. Hagen, *Chem. Ing. Tech.* **2011**, *83 (7)*, 965–978. DOI: https://doi.org/10.1002/cite.201100014

[22] M. Mickler, H.-J. Bart, *Chem. Ing. Tech.* **2013**, *85 (6)*, 901–906. DOI: https://doi.org/10.1002/cite.201200139

[23] M. Lichti, C. Roth, H.-J. Bart, *EP 3 067 685 A1*, **2016**.

[24] M. Lichti, *Optische Erfassung von Partikelmerkmalen: Entwicklung einer Durchlichtmesstechnik für Apparate der Fluidverfahrenstechnik*, Dissertation, TU Kaiserslautern **2018**.

[25] J. Steinhoff, E. Charlafti, L. Reinecke, M. Kraume, H.-J. Bart, *Can. J. Chem. Eng.* **2020**, *98 (1)*, 384–393. DOI: https://doi.org/10.1002/cjce.23603

[26] M. Mickler, *Inline-Analyse, Simulation und Vorhersage von flüssigen Mehrphasenströmungen in Extraktionskolonnen*, Dissertation, TU Kaiserslautern **2014**.

[27] P. Schmitt, M. W. Hlawitschka, H.-J. Bart, *Chem. Ing. Tech.* **2020**, *262 (4)*, 12215. DOI: https://doi.org/10.1002/cite.201900105

[28] M. Lichti, H.-J. Bart, *Flow Meas. Instrum.* **2018**, *60*, 164–170.

[29] D. Wirz, M. Lichti, H.-J. Bart, *Chem. Ing. Tech.* **2018**, *90 (9)*, 1318.

[30] J. Schulz, H.-J. Bart, *Chem. Eng. Res. Des.* **2019**, *147*, 624–633. DOI: https://doi.org/10.1016/j.cherd.2019.05.041

[31] M. Lichti, J. Schulz, H.-J. Bart, *Chem. Ing. Tech.* **2019**, *91 (4)*, 429–434. DOI: https://doi.org/10.1002/cite.201800045

[32] M. Asadollahzadeh, R. Torkaman, M. Torab-Mostaedi, J. Safdari, *Chem. Eng. Res. Des.* **2017**, *117*, 648–658.

[33] H. Yi, Y. Wang, K. H. Smith, W. Y. Fei, G. W. Stevens, *Ind. Eng. Chem. Res.* **2017**, *56 (4)*, 999–1007.

[34] T. Xie, Y. Gao, W. Liu, *AIChE J.* **2015**, *61 (11)*, 3958–3963.

[35] M. Gholam Samani, A. Haghighi Asl, J. Safdari, M. Torab-Mostaedi, *Chem. Eng. Res. Des.* **2012**, *90 (12)*, 2148–2154.

[36] M. Torab-Mostaedi, J. Safdari, F. Torabi Hokmabadi, F. Hokmabadi, *Iran. J. Chem. Eng.* **2011**, *8 (4)*, 3–10.

[37] M. R. Usman, H. Sattar, S. N. Hussain, H. Muhammad, A. Asghar, W. Afzal, *Chem. Eng. Sci.* **2009**, *26 (4)*, 677–683.

[38] T. Steinmetz, *Tropfenpopulationsbilanzgestütztes Auslegungsverfahren zur Skalierung einer gerührten Miniplant-Extraktionskolonne*, Fortschritt-Berichte VDI Reihe 3, Verfahrenstechnik, Vol. 885, VDI-Verlag, Düsseldorf **2007**.

[39] M. Lorenz, H. Haverland, A. Vogelphol, *Chem. Eng. Technol.* **1990**, *13 (1)*, 411–422.

[40] W. J. Korchinsky, R. Al-Husseini, *J. Chem. Technol. Biotechnol.* **1986**, *36 (9)*, 395–409. DOI: https://doi.org/10.1002/jctb.280360903

[41] M. O. Garg, H. R. C. Pratt, *AIChE J.* **1984**, *30 (3)*, 432–441.

[42] J. Schäfer, P. Schmitt, M. W. Hlawitschka, H.-J. Bart, *Chem. Ing. Tech.* **2019**, *91 (11)*, 1688–1695. DOI: https://doi.org/10.1002/cite.201900099

[43] O. Ronneberger, P. Fischer, T. Brox, *U-Net: Convolutional Networks for Biomedical Image Segmentation*, arXiv:1505.04597v1, **2015**.

[44] N. Maiti, U. B. Desai, A. K. Ray, *Thin Solid Films* **2000**, *376 (1–2)*, 16–25. DOI: https://doi.org/10.1016/S0040-6090(00)01396-1

[45] H.-J. Bart, M. Mickler, H. Jildeh, in *Optical Imaging: Technology, Methods and Applications* (Eds: A. Tanaka, B. Nakamura), Nova Publishers, N.Y. Lancaster **2012**.

[46] P. L. Rosin, *Graph. Model. Image Process.* **1999**, *61 (5)*, 245–259. DOI: https://doi.org/10.1006/gmip.1999.0500

[47] H. B. Jildeh, M. W. Hlawitschka, M. Attarakih, H.-J. Bart, Solution of Inverse Problem with the One Primary One Secondary Particle Model (OPOSPM) Coupled with Computational Fluid Dynamics (CFD), *Procedia Eng.* **2012**, *42*, 1692–1710.

[48] H. B. Jildeh, *Liquid-liquid extraction columns*, Dissertation, TU Kaiserslautern **2015**.

[49] H.-J. Bart, H. Jildeh, M. Attarakih, *Solvent Extr. Ion Exch.* **2020**, *38 (1)*, 14–65. DOI: https://doi.org/10.1080/07366299.2019.1691136

[50] M. Attarakih, M. Jaradat, C. Drumm, H.-J. Bart, S. Tiwari, V. K. Sharma, in *19th European Symposium on Computer Aided Process Engineering – ESCAPE19* (Eds: J. Jeżowski, J. Thullie), Elsevier, Amsterdam **2009**.

[51] G. Kocamustafaogullari, M. Ishii, *Int. J. Heat Mass Transfer* **1995**, *38 (3)*, 481–493. DOI: https://doi.org/10.1016/0017-9310(94)00183-V

[52] M. W. Hlawitschka, *Computational fluid dynamics aided design of stirred liquid-liquid extraction columns*, Dissertation, TU Kaiserslautern **2013**.

[53] A. Vignes, Hydrodynamique des Dispersions – Mouvement d'un globule dans un fluide immobile et infini, *Genie Chim.* **1965**, *93*, 129–142.

[54] A. Klee, R. Treybal, Rate of rise or fall of liquid drops, *AlChE J.* **1956**, *2*, 444–447.

[55] J. Grace, T. Wairegi, T. Nguyen, Shapes and velocities of single drops and bubbles moving freely through immiscible liquids, *Trans. Inst. Chem. Eng.* **1976**, *54*, 167–173.

[56] J. Fang, J. C. Godfrey, Z.-Q. Mao, M. J. Slater, C. Gourdon, *Chem. Eng. Technol.* **1995**, *18 (1)*, 41–48. DOI: https://doi.org/10.1002/ceat.270180109

[57] G. Modes, *Grundsätzliche Studie zur Populationsdynamik einer Extraktionskolonne auf Basis von Einzeltropfenuntersuchungen*, Berichte aus der Verfahrenstechnik, Shaker, Aachen **2000**.

[58] S. A. Schmidt, *Populationsdynamische Simulation gerührter Extraktionskolonnen auf der Basis von Einzeltropfen- und Tropfenschwarmuntersuchungen*, Berichte aus der Verfahrenstechnik, Shaker, Aachen **2006**.

[59] D. Garthe, *Fluiddynamics and mass transfer of single particles and swarms of particles in extraction columns*, Verfahrenstechnik, Dr. Hut, München **2006**.

[60] S. A. Schmidt, *Populationsdynamische Simulation gerührter Extraktionskolonnen auf der Basis von Einzeltropfen- und Tropfenschwarmuntersuchungen*, Dissertation, TU Kaiserslautern **2006**.

[61] J. S. Heine, H.-J. Bart, *Can. J. Chem. Eng.* **2019**, *27*, 203. DOI: https://doi.org/10.1002/cjce.23685

[62] F. Garner, M. Tayeban, The Importance Of The Wake In Mass Transfer From Both Continuous And Dispersed Phase Systems, *An. R. Soc. Esp. Fis. Quim., Ser. B.* **1960**, *56*, 479–490.

[63] R. Kronig, J. Brink, On the theory of extraction from falling droplets, *Appl. Sci. Res.* **1951**, *2*, 142–154.

[64] R. Treybal, *Liquid extraction*, McGraw-Hill, New York **1963**.

[65] P. M. Heertjes, W. A. Holve, H. Talsma, *Chem. Eng. Sci.* **1954**, *3 (3)*, 122–142. DOI: https://doi.org/10.1016/0009-2509(54)80017-0

[66] J. C. Bonnet, G. V. Jeffreys, *J. Chem. Tech. Biotechnol.* **1983**, *33 (4)*, 176–186. DOI: https://doi.org/10.1002/jctb.504330403

[67] C. Korb, A. Keller, H.-J. Bart, *Chem. Eng. Technol.* **2018**, *41 (11)*, 2212–2222. DOI: https://doi.org/10.1002/ceat.201800239

[68] N. S. Kolhe, Y. H. Mirage, A. V. Patwardhan, V. K. Rathod, N. K. Pandey, U. K. Mudali, R. Natarajan, *Chem. Eng. Res. Des.* **2011**, *89 (10)*, 1909–1918. DOI: https://doi.org/10.1016/j.cherd.2011.01.020

[69] K. Nishi, J. M. Perera, R. Misumi, M. Kaminoyama, G. W. Stevens, *J. Chem. Eng. Jpn.* **2010**, *43 (4)*, 342–348. DOI: https://doi.org/10.1252/jcej.09we175

[70] A. B. Jahya, G. W. Stevens, H. R. C. Pratt, *Solvent Extr. Ion Exch.* **2009**, *27 (1)*, 63–82. DOI: https://doi.org/10.1080/07366290802544734

[71] M. Torab-Mostaedi, J. Safdari, *J. Chem. Eng. Japan* **2009**, *26 (4)*, 685–694. DOI: https://doi.org/10.1590/S0104-66322009000400007

[72] C. Tsouris, L. L. Tavlarides, *Chem. Eng. Sci.* **1993**, *48 (24)*, 4097–4104. DOI: https://doi.org/10.1016/0009-2509(93)80254-N

[73] M. W. Hlawitschka, M. M. Attarakih, S. S. Alzyod, H.-J. Bart, *Chin. J. Chem. Eng.* **2016**, *24 (2)*, 259–263. DOI: https://doi.org/10.1016/j.cjche.2015.07.023

[74] M. Attarakih, M. W. Hlawitschka, M. Abu-Khader, S. Al-Zyod, H.-J. Bart, *Appl. Math. Modell.* **2015**, *39 (17)*, 5105–5120. DOI: https://doi.org/10.1016/j.apm.2015.04.006

[75] S. Charton, M. Thebault, S. Winn, H. Roussel, F. Lamadie, M. W. Hlawitschka, C. Korb, H.-J. Bart, *Chem. Eng. Res. Des.* **2017**, *125*, 483–493. DOI: https://doi.org/10.1016/j.cherd.2017.07.033

[76] M. Mickler, H. B. Jildeh, M. Attarakih, H.-J. Bart, *Can. J. Chem. Eng.* **2014**, *92 (2)*, 307–317. DOI: https://doi.org/10.1002/cjce.21893

[77] H. B. Jildeh, M. Attarakih, M. Mickler, H.-J. Bart, *Can. J. Chem. Eng.* **2014**, *92 (2)*, 210–219. DOI: https://doi.org/10.1002/cjce.21892

[78] H.-J. Bart, M. Grünewald, J.-U. Repke, S. Scholl, *Chem. Ing. Tech.* **2020**, *92 (7)*, in press. DOI: https://doi.org/10.1002/cite.202000037